Electronic Supplementary Information (ESI)

Designing the new aluminium muconate metal-organic framework (MIL-53-muc) as methanol adsorbent for sub-zero temperature heat transformation applications

Tobie J. Matemb Ma Ntep,[a] Helge Reinsch,[b] Philipp P. C. Hügenell,[c] Sebastian-Johannes Ernst,[c] Emrah Hastürk,[a] and Christoph Janiak *[a]

[a] Institut für Anorganische Chemie und Strukturchemie, Heinrich-Heine-Universität Düsseldorf, Universitätsstraße 1, D- 40225 Düsseldorf, Germany

[b] Institut für Anorganische Chemie, Christian-Albrechts-Universität zu Kiel, Max-Eyth-Straße 2, 24118 Kiel, Germany

[c] Fraunhofer Institue for Solar Enegy Systems (ISE), Heidenhofstraße 2, 79110 Freiburg, Germany

* Corresponding author: E-mail: janiak@uni-duesseldorf.de; Fax: + 49-211-81-12287; Tel: +49-211-81-12286
Additional email addresses:
tobie.matemb.ma.ntep@uni-duesseldorf.de; hreinsch@ac.uni-kiel.de; philipp.huegenell@ise.fraunhofer.de; sebastian-johannes.ernst@ise.fraunhofer.de; emrah.hastuerk@hhu.de;

Table of contents

Synthesis details

In order to obtain a muconate-based Al-MOF with MIL-53 structure, the initial syntheses were conducted by a conventional solvothermal route (without stirring) in a programmable oven and by microwave-assisted solvothermal heating using $Al_2(SO_4)_3 \cdot 18H_2O$ as the metal source in a H_2O/DMF solvent mixture. The choice of this salt was guided by the result previously obtained by Reinsch *et al.* for the synthesis of a MIL-53 type Al-MOF using the aliphatic adipate linker, which is close to the muconate linker.[1] We then realized that the targeted product was obtained under microwave conditions (under stirring). From the conventional solvothermal route in a programmable oven the product was mixed with an amorphous phase. For further trials in order to obtain the material also under solvothermal conditions in the oven, $Al(NO_3)_3 \cdot 9H_2O$ was used in place of $Al_2(SO_4)_3 \cdot 18H_2O$, which then yielded the pure expected phase of MIL-53-muc.

Infrared and Raman spectroscopy of MIL-53-muc and Aluminium fumarate

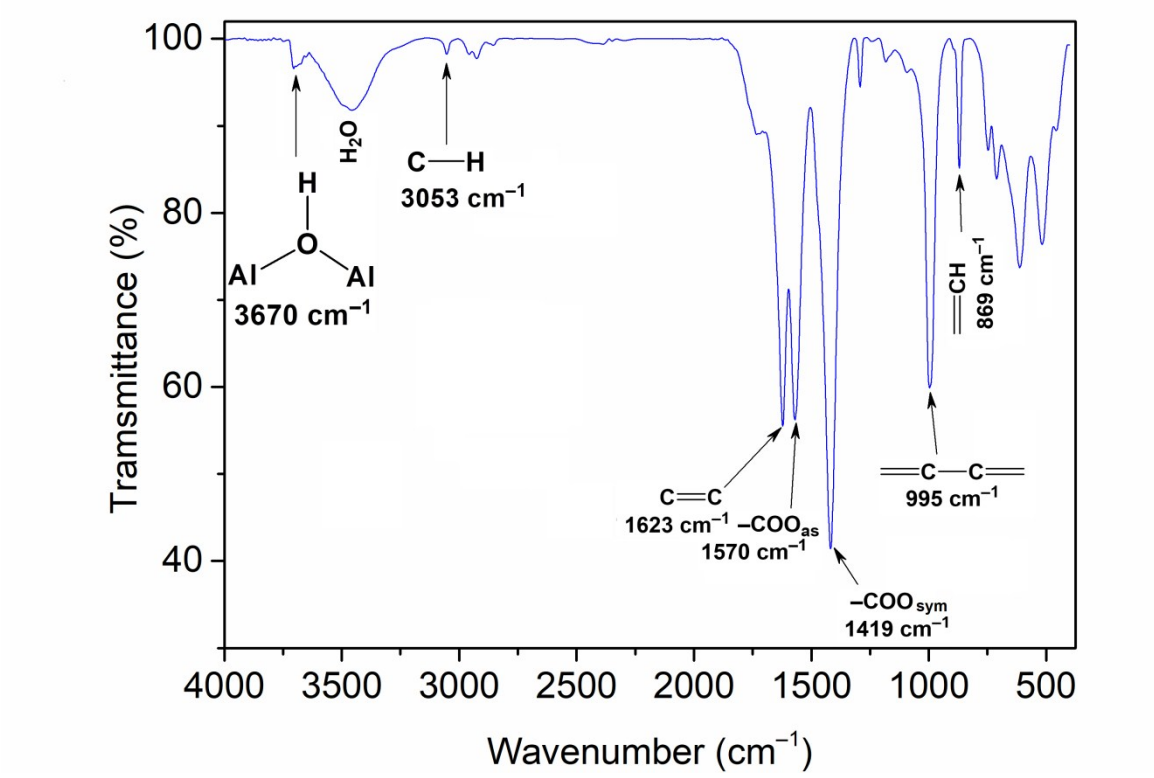

Fig. S1 Infrared spectrum of MIL-53-muc.

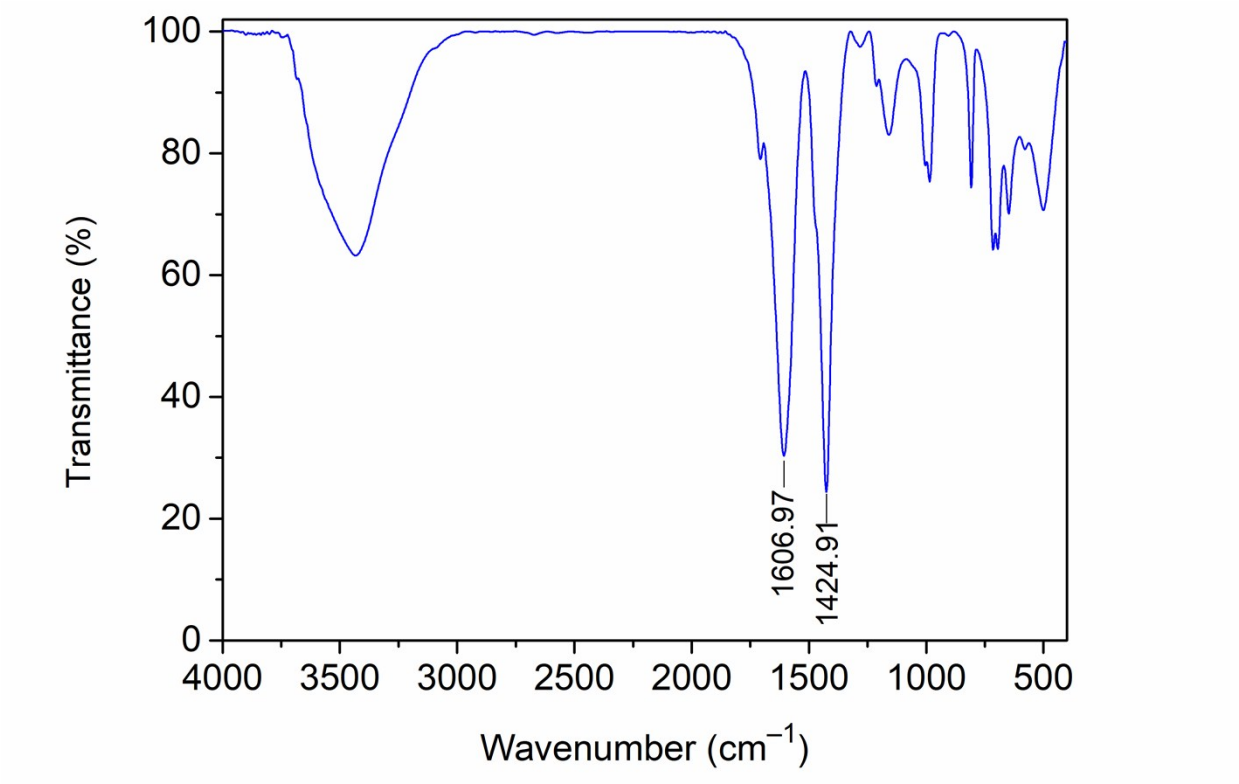

Fig. S2 Infrared spectrum of aluminium fumarate (Al-Fum).

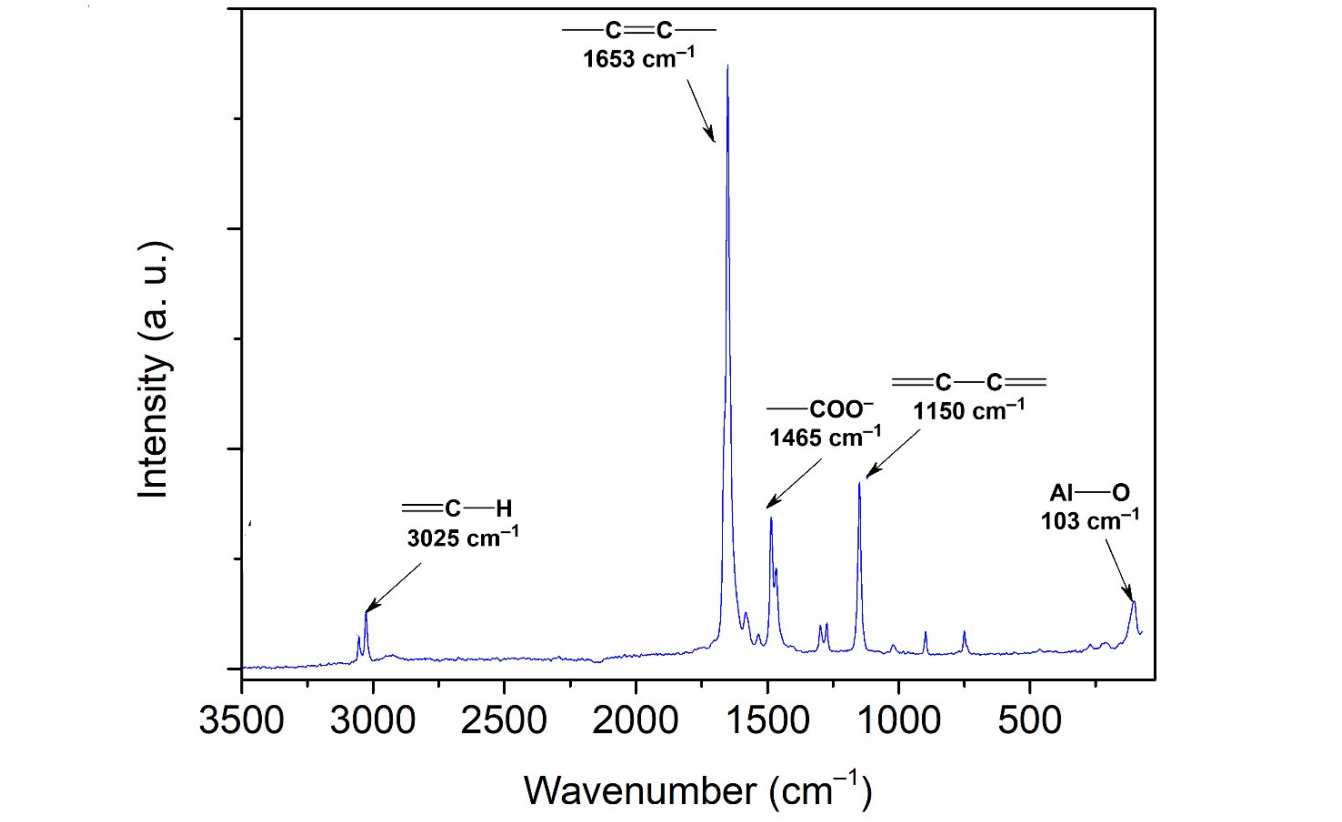

Fig. S3 Raman spectrum of MIL-53-muc.

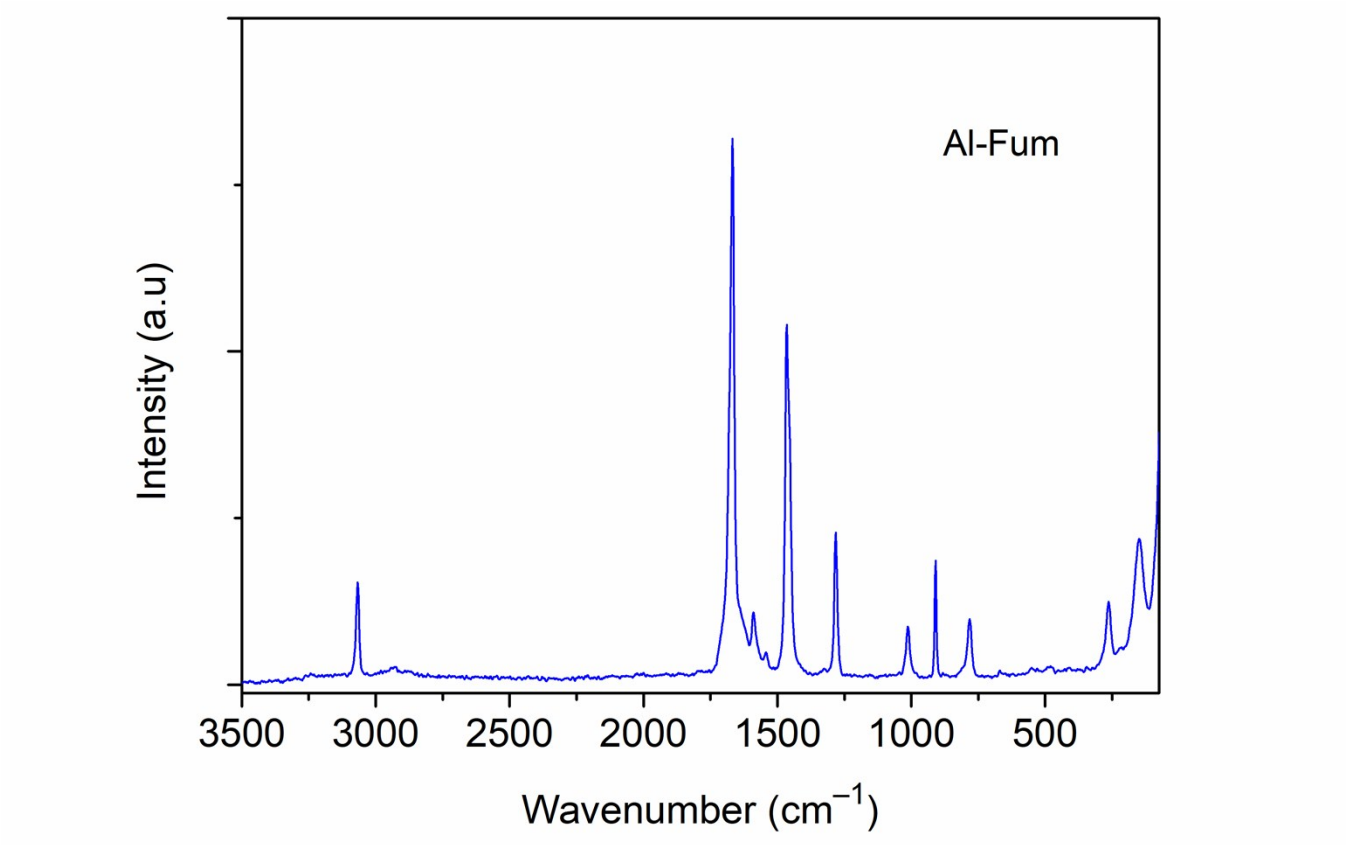

Fig. S4 Raman spectrum of aluminium fumarate.

Structure modelling and elucidation of MIL-53-muc

Except for the special position of several atoms, no parameters were fixed. The refined parameters comprise the non-special positions for the Al-O chains, the translational and rotational motion of the rigid body linker fragment as well as the position and occupancy of the atoms representing the occluded solvent molecules. Moreover, the cell parameters and general temperature factor were refined. These structural parameters aside, the background was modelled by a 12th order polynomial. Of course, the refinement included a peak shape function (Pseudo-Voigt), a scale factor and a zero error, and as described in the manuscript a preferred orientation was also modelled.

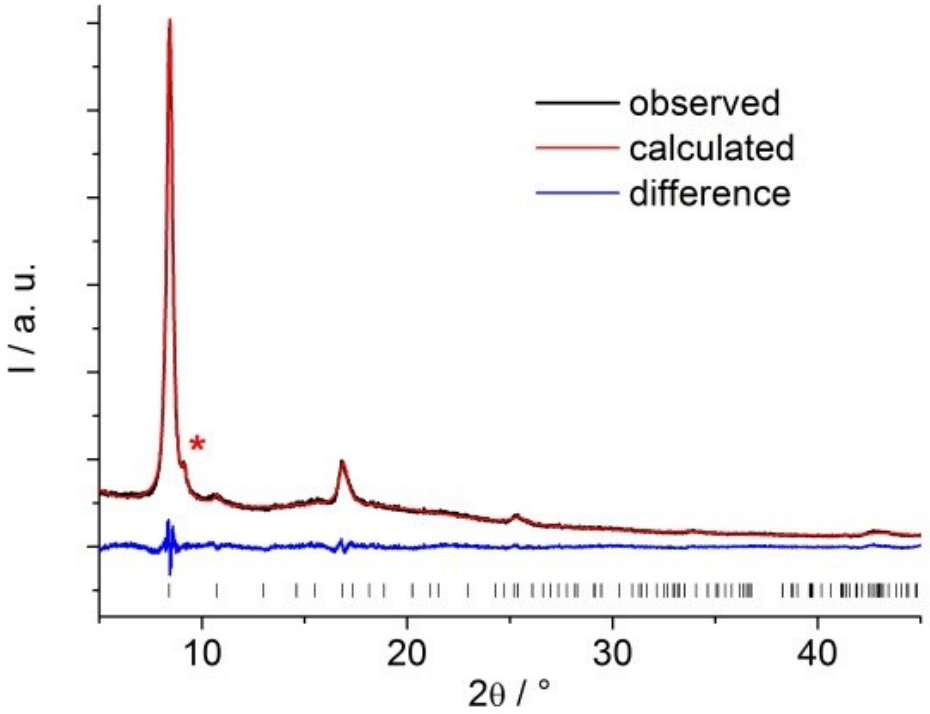

Fig. S5a Final Rietveld plot for MIL-53-muc. The black line represents measured data, the red line is the fit and the blue line indicates the difference curve. Vertical bars indicate the allowed peak positions. The red asterisk marks the shoulder of the first peak, attributed to a crystalline impurity.

Table S1 Selected relevant structure parameters for MIL-53-muc.

Compound	MIL-53-muc
Formula sum	[Al(OH) (O_2C-C_4H_4-CO_2)]
Space group	*C*2/m
Crystal system	monoclinic
Cell parameters	*a* = 14.71(3) Å
	b = 16.51(2) Å
	c = 6.53(2) Å
	α = 90°
	β = 68.1(2)°
	γ = 90°
R_{WP}	4.1 %
GoF	2.6
R_{Bragg}	0.3 %

Crystallographic Information File

```
data_structure
_symmetry_cell_setting          monoclinic
_symmetry_space_group_name_H-M   'C 2/m'
_symmetry_Int_Tables_number      12
_space_group_name_Hall          '-C 2y'
loop_
_symmetry_equiv_pos_site_id
_symmetry_equiv_pos_as_xyz
1 x,y,z
2 -x,y,-z
3 x,-y,z
4 -x,-y,-z
5 1/2+x,1/2+y,z
6 1/2-x,1/2+y,-z
7 1/2+x,1/2-y,z
8 1/2-x,1/2-y,-z
_cell_length_a                  14.71(3)
_cell_length_b                  16.513(18)
_cell_length_c                  6.535(18)
_cell_angle_alpha               90
_cell_angle_beta                68.1(2)
_cell_angle_gamma               90
_cell_volume                    1472.84
loop_
_atom_site_label
_atom_site_type_symbol
_atom_site_fract_x
_atom_site_fract_y
_atom_site_fract_z
Al1 Al 0 -0.5 -0.5
Al2 Al 0 -0.5 0
O1 O 0.062(10) -0.5 -0.30(5)
O2 O -0.09485 -0.42342 0.00103
O3 O -0.09845 -0.41843 -0.33648
C1 C -0.13045 -0.39935 -0.13705
C2 C -0.2162 -0.34879 -0.06949
C3 C -0.21942 -0.28117 0.03508
G1 O -0.62(4) -0.5 -0.1(2)
G2 O -0.58(3) -0.5 -0.5
```

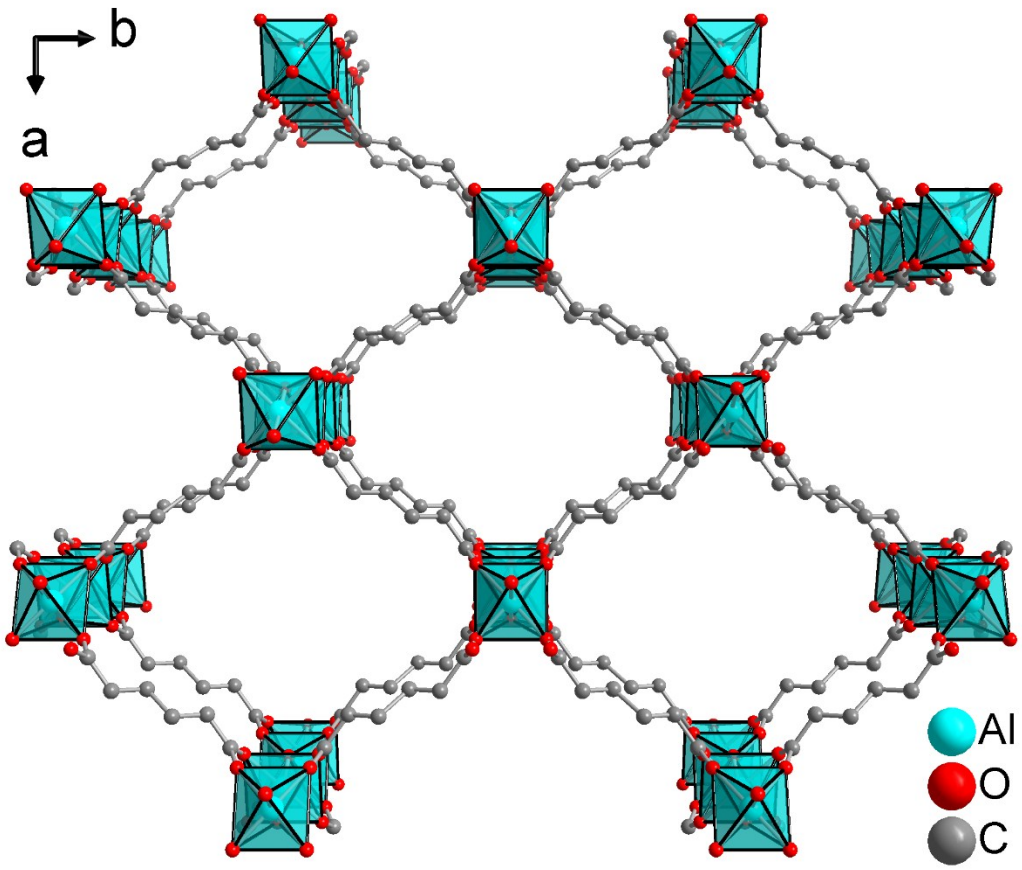

Fig. S5b Extended section of the packing diagram in the structure of MIL-53-muc (guest molecules are not shown and hydrogen atoms were not included in the Rietveld refinement).

Thermogravimetric analysis (TGA)

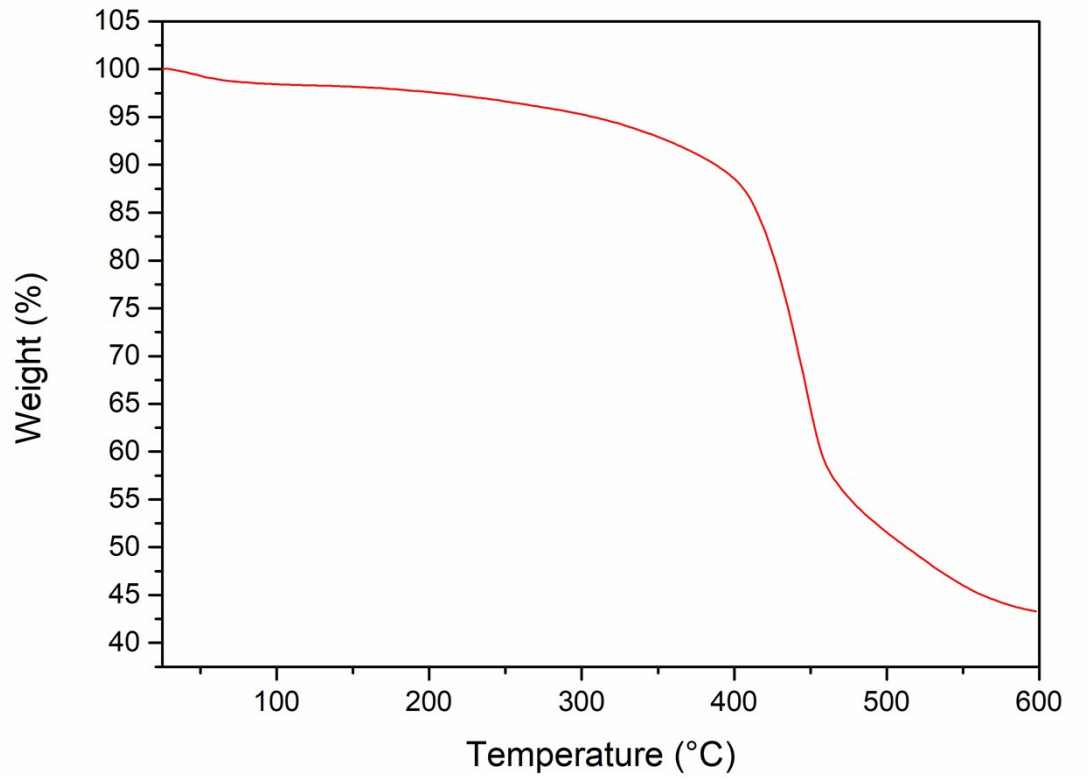

Fig. S6 Trace of thermogravimetry analysis conducted under air for MIL-53-muc.

PXRD patterns of the chemical stability testing

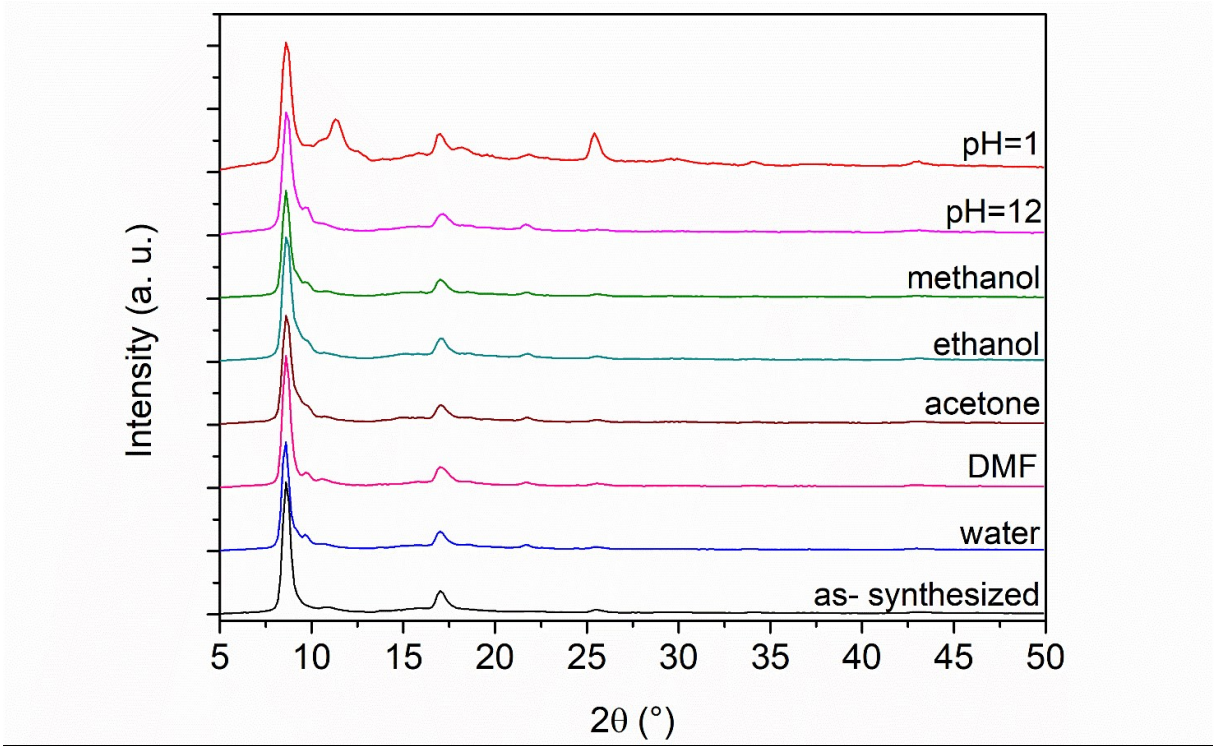

Fig. S7 PXRD patterns of MIL-53-muc after stirring 24 h at room temperature in various solvents and solutions.

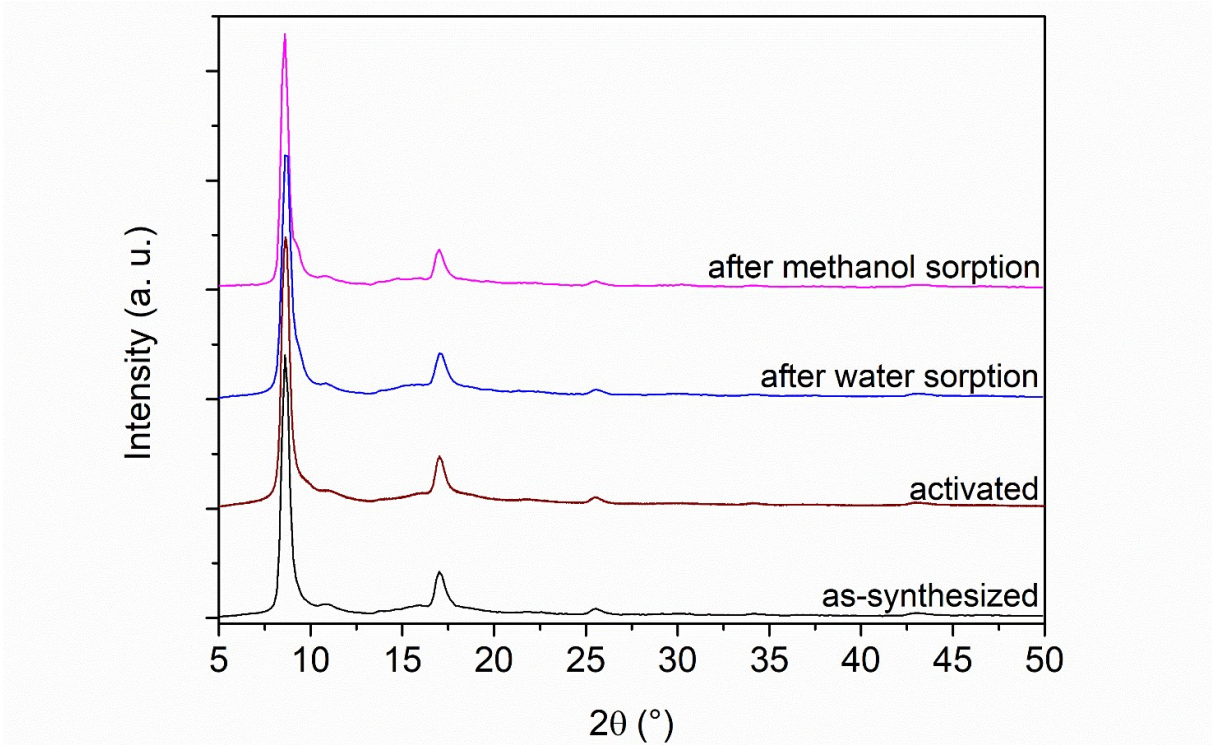

Fig. S8 PXRD patterns of MIL-53-muc after outgassing and after vapour sorption.

Nitrogen sorption and porosity analysis

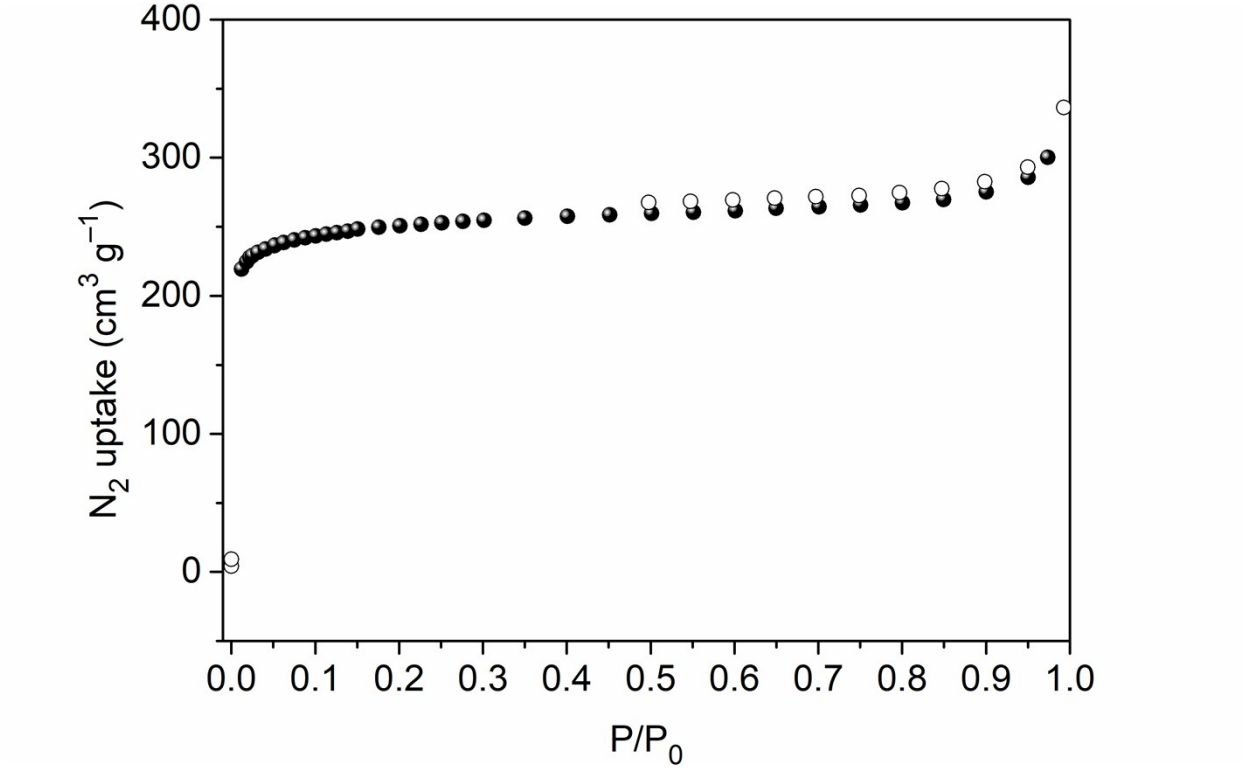

Fig. S9 Nitrogen sorption isotherms for aluminium fumarate (filled symbols: adsorption; empty symbols: desorption).

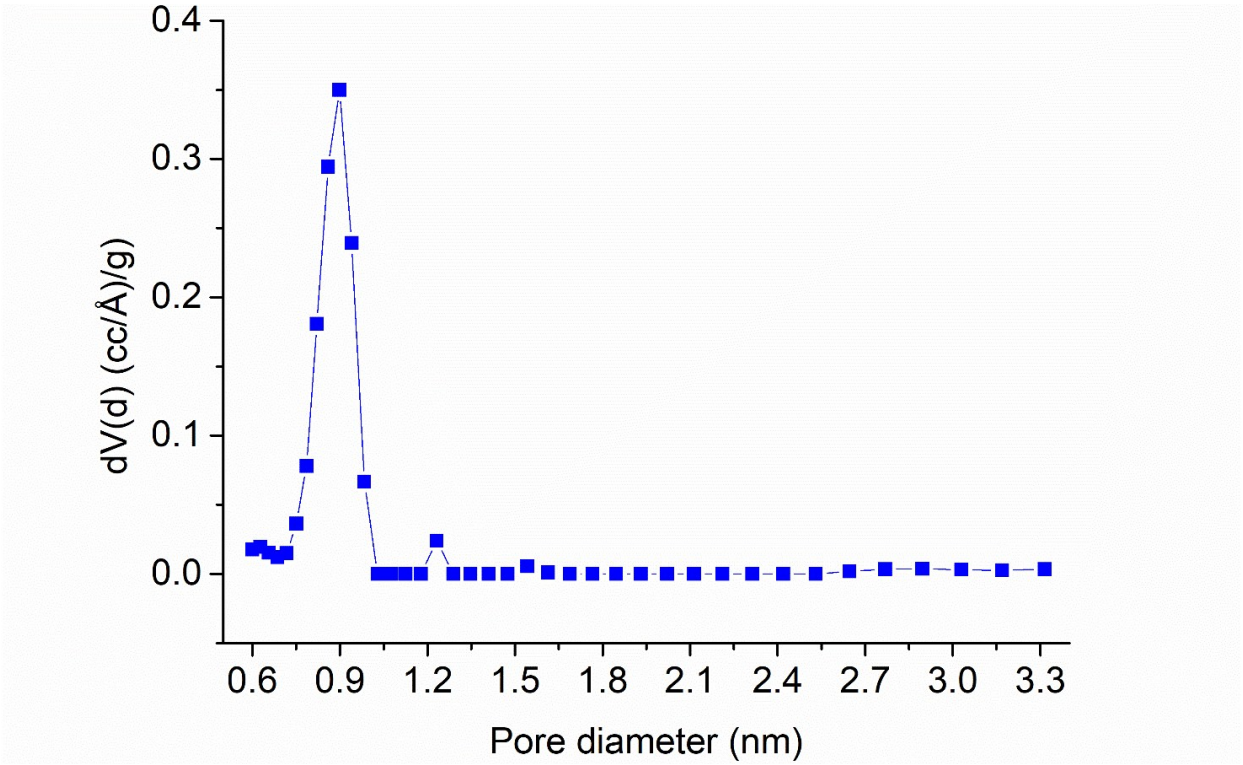

Fig. S10 Pore size distribution analysis for MIL-53-muc from N_2 sorption isotherm with the NLDFT model.

Table S2 Porosity parameters of MIL-53-muc

Materials	S_{BET} (m^2g^{-1}) [a]	$S_{micro\text{-}BET}$ (m^2g^{-1}) [b]	S_{Ext} (m^2g^{-1}) [c]	$V_{pore\ (total)}$ (cm^3g^{-1}) [d]	$V_{pore\ (micro)}$ (cm^3g^{-1}) [e]
MIL-53-Muc	1750	1530	220	0.72	0.52
Al-Fum	982	864	118	0.42	0.33

[a] BET surface areas (S_{BET}) were obtained from five adsorption points in the pressure range PP_0^{-1}=0.001-0.05. [b] Micropore areas ($S_{micro\text{-}BET}$) were obtained by t-plot and V-t-method. [c] External area (S_{Ext}) refers to all area that does not originate from micropores and it includes meso- and macropores, i.e. pores > 2nm. Obtained by t-plot and V-t-method. [d] Total pore volumes ($V_{pore\ (total)}$) were derived at PP_0^{-1}= 0.95 for pores ≤ 20 nm. [e] Micropore volume ($V_{pore\ (micro)}$) refers to volume that originates only from micropores, obtained by V-t-method with thickness method 'DeBoer'. All correlation coefficients (r) in calculations were >0.999.

Multicycle adsorption-desorption stability tests

We would like to note that the water sorption isotherms in Fig. S11 (for a five-cycle water sorption stability test) were conducted with a sample obtained under slightly different synthesis conditions. This has resulted in a smaller hysteresis loop, indicating that the extent of the hysteresis (or the flexibility) depends on the synthetic route. This aspect is included in our current investigations and was already reported for the parent MIL-53-BDC. However, we do not expect the stability in itself to be different from the product obtained under our optimized synthesis.

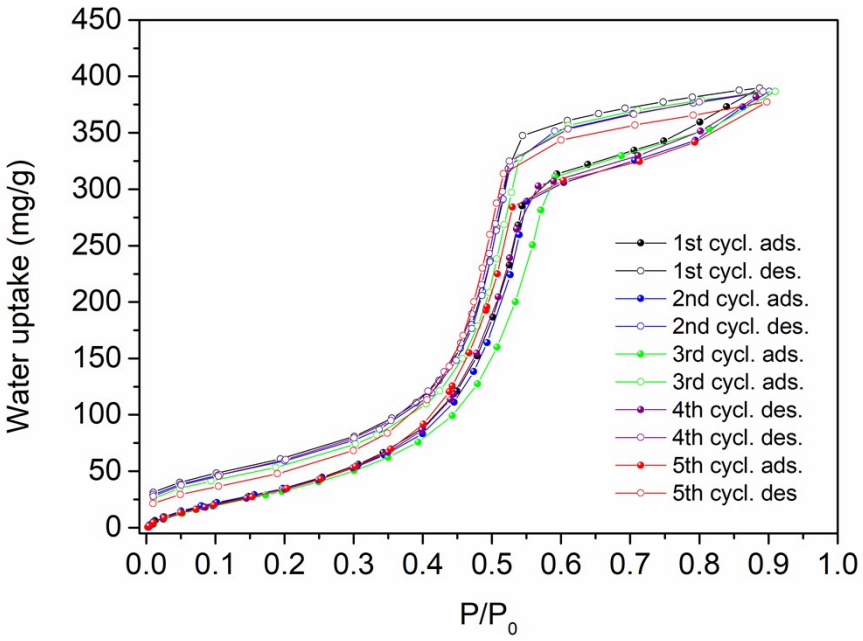

Fig. S11 Water sorption isotherms for MIL-53-muc, collected for five consecutive cycles. The water uptake capacity indicates the hydrolytic stability of MIL-53-muc.

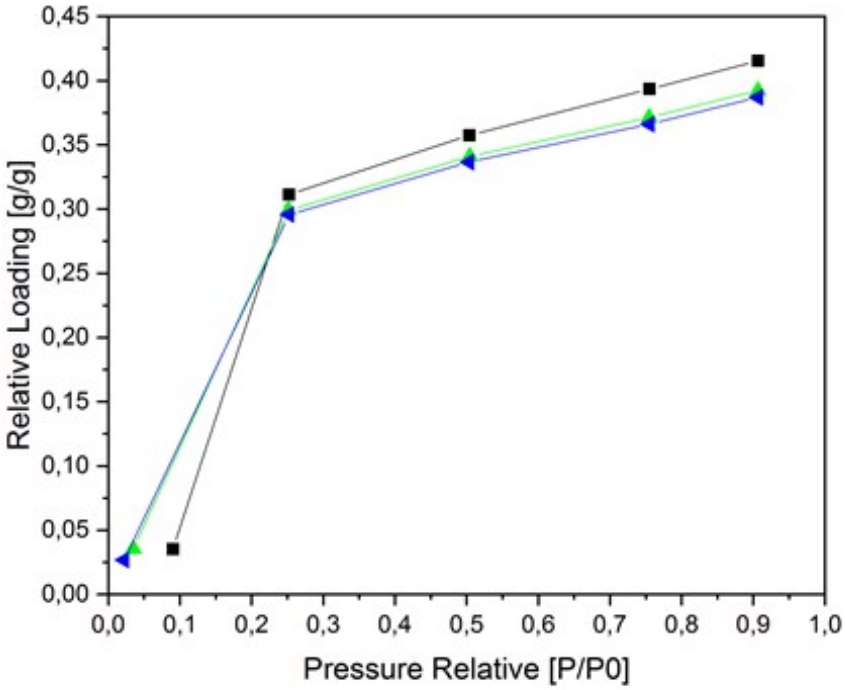

Fig. S12 Methanol adsorption isotherms measured after multicycle adsorption-desorption stability test. The black squares show the equilibrium points of the untreated sample MIL-53-muc. The green triangles correspond to the equilibrium points after 25 cycles and the blue triangles after 50 cycles.

Experimental

The 50-cycle stability in water vapor sorption was examined in a Setaram™ TGA-DSC-111. A humidified argon gas flow (40 °C, 76.3% relative humidity) was generated by a Setaram™ WetSys humidity controller and passed through the sample chamber, while the temperature of the sample chamber itself was varied. For multi-cycle ad-/desorption experiments, the temperature of the sample chamber was varied between 40 °C and 140 °C with a cycle time of 5 h for 50 cycles. Prior to and after the cycles, the sample was dried at 140 °C in a dry gas flow and then humidified.

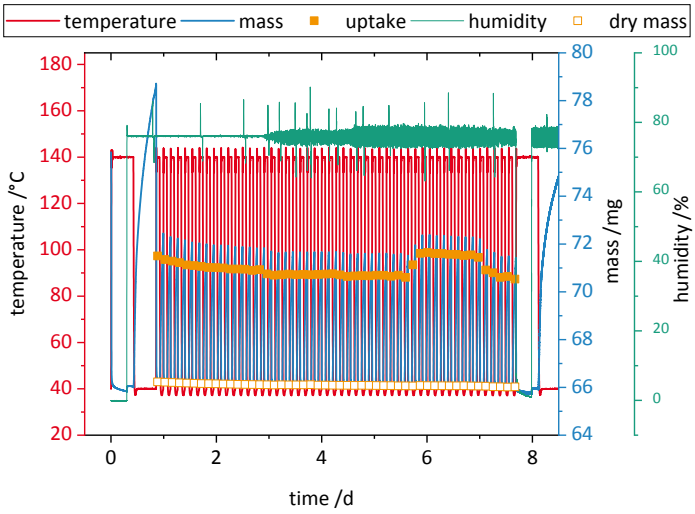

Fig. S13 50 cycles of adsorption and desorption of MIL-53-muc in a thermogravimetric analyzer. Red curve: temperature, blue curve: sample mass, green curve: humidity, filled orange squares: uptake, open orange squares: dry mass.

The cycle experiment whose results are depicted in Fig. S13 shows that the sample keeps its ability to adsorb water vapor over at least 50 cycles, though a small decrease of -1.3 % can be observed (orange squares). Further, the dry mass of the sample (open orange squares) stays pretty constant (-0.3 mass-%). Although the water vapor was slightly inconstant over the second half of the experiment, it is proven, that MIL-53-muc is not unstable in a humid atmosphere and over at least 50 cycles.

Isosteric heat of water and methanol adsorption

Making use of isotherms collected at three different temperatures (see Fig. S12 for water and Fig. 13 for methanol), the isosteric heat of adsorption was finally calculated by applying the Clausius-Clapeyron equation (eq. 1).

$$Q_{st} = -R\left(\frac{T_2 T_1}{T_2 - T_1}\right) ln\frac{P_2}{P_1} \qquad (1)$$

Q_{st} is the isosteric heat of adsorption (kJ mol^{-1}); T_1 and T_2 are two different temperatures at which isotherms are measured (K); P_1 and P_2 are two pressures at T_1 and T_2 respectively, corresponding to the same isostere (the same uptake).

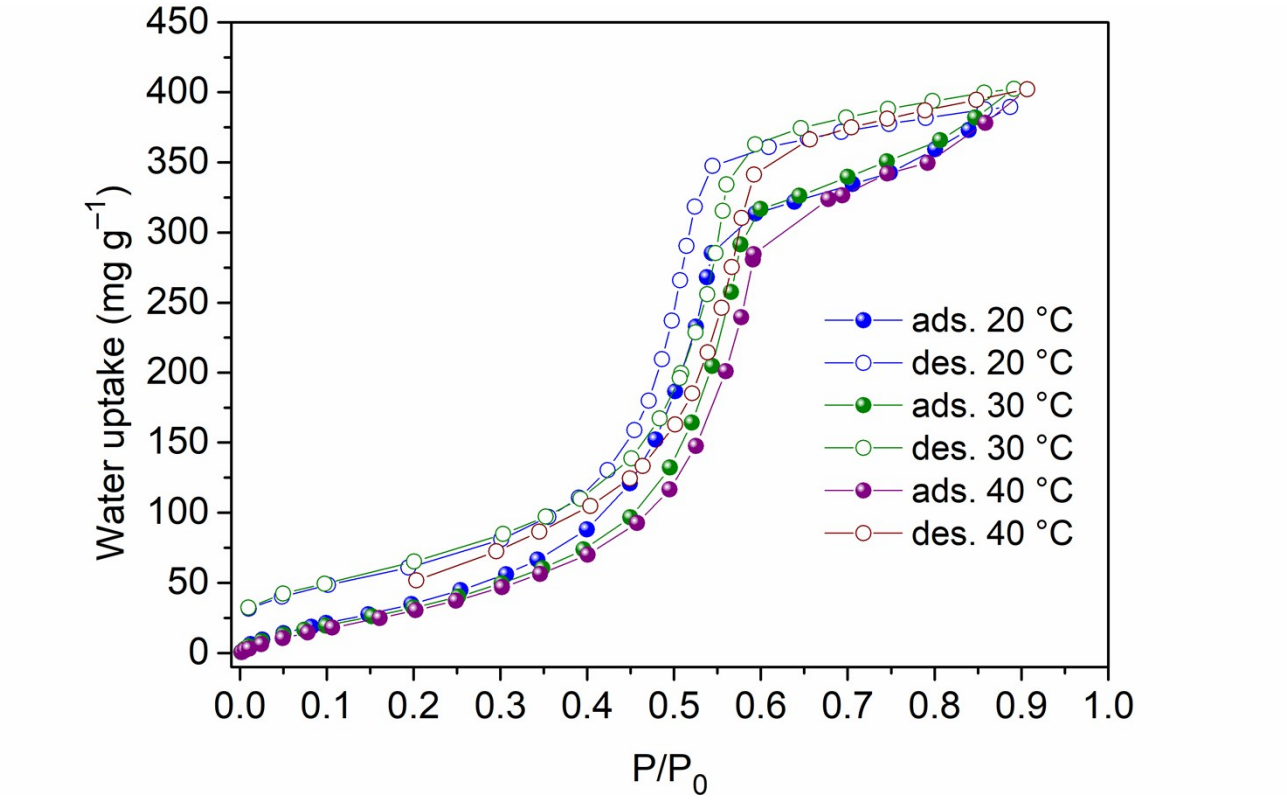

Fig. S14 Water sorption isotherms for MIL-53-muc collected at three different temperatures. On the page "Response to Review" please provide a separate point-by-point response to all comments in the collated report.

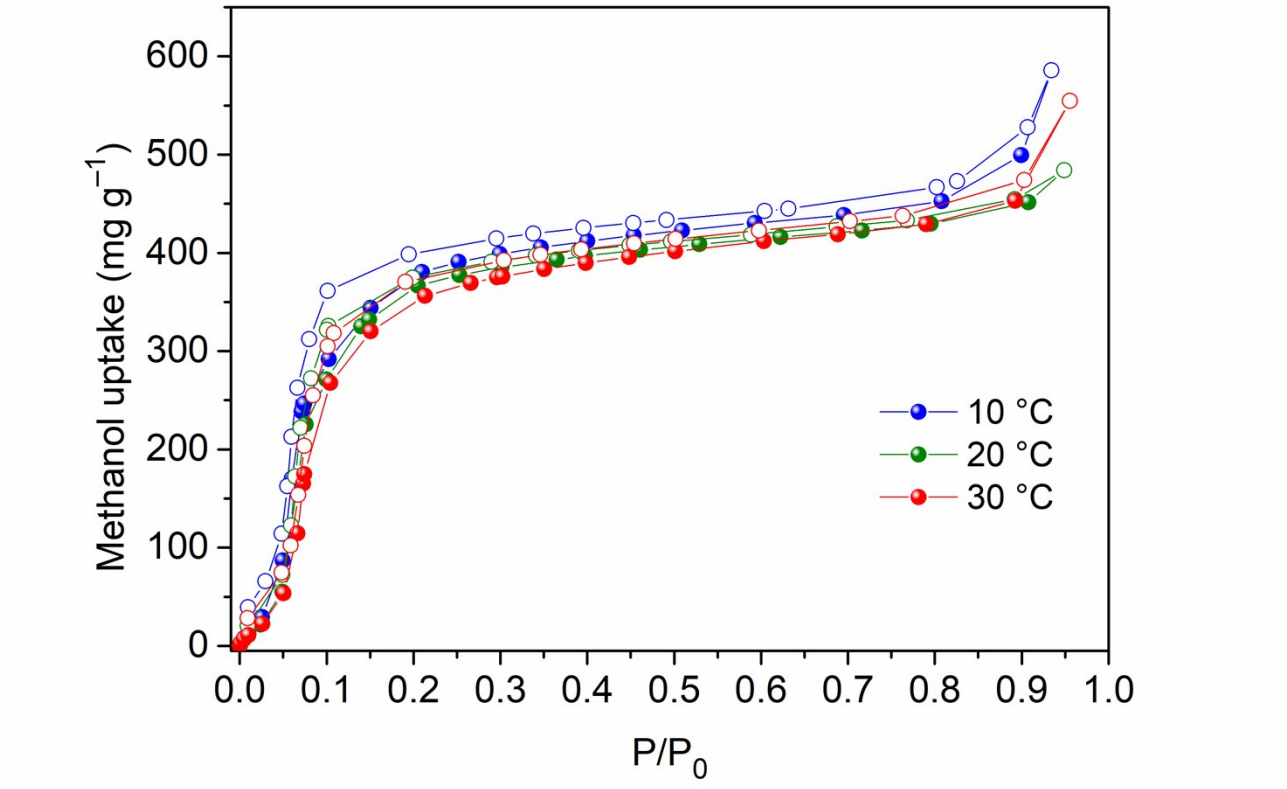

Fig. S15 Methanol sorption isotherms for MIL-53-muc, collected at three temperatures: 10 °C (blue), 20 °C (green) and 30 °C red (red).

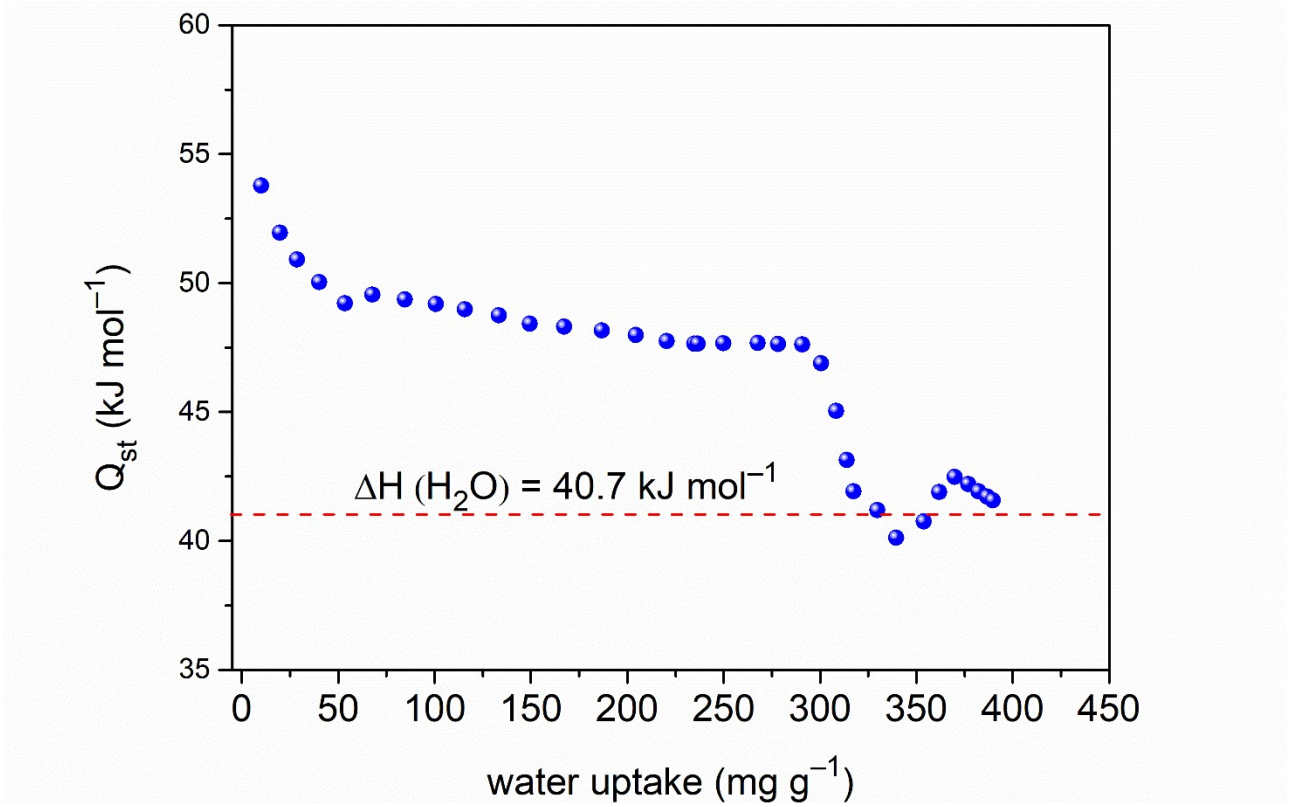

Fig. S16 Plot of the isosteric heat of water adsorption for MIL-53-muc.

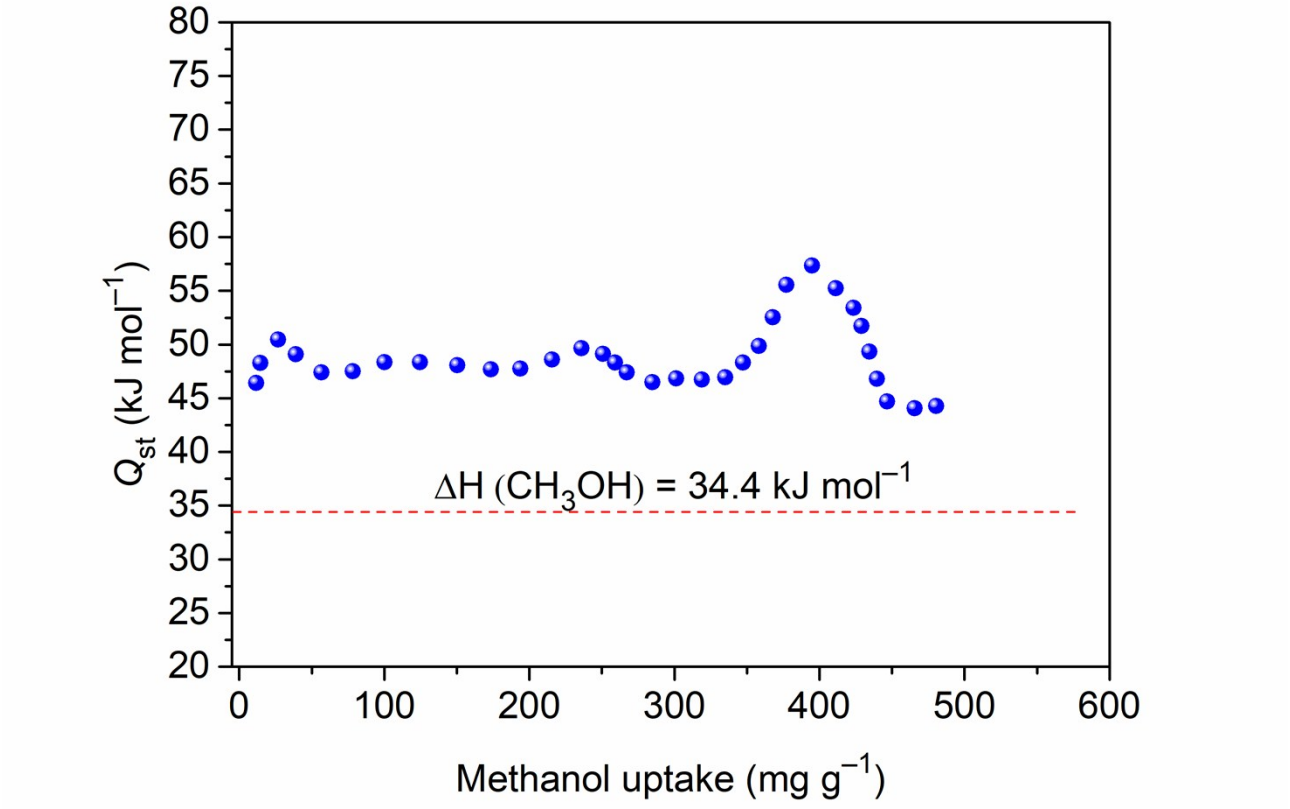

Fig. S17 Plot of the isosteric heat of methanol adsorption for MIL-53-muc.

Calculation of the heat storage capacity C_{HS} for MIL-53-muc

$$C_{HS} = \frac{\Delta H_{ads} \cdot \Delta w}{M_w} \qquad (2)$$

where ΔH_{ads} is the heat of water adsorption, Δw is the working capacity and M_w is the molar weight of methanol.

Calculations of methanol sorption performance for AHP and TDC applications

To assess the potential of the MIL-53-muc sample in adsorption heat transformation, the measured methanol adsorption data were fitted using a weighted-dual site Langmuir approach (wDSL).

$$X(p,T) = X_L(1 - w(p,T)) + X_U(p,T)w(p,T) \qquad (3)$$

$$X_L(p,T) = X_{L,\infty}\frac{b_L p}{1 + b_L p} \qquad (4)$$

$$X_U(p,T) = X_{U,\infty}\frac{b_U p}{1 + b_U p} + b_H p \qquad (5)$$

$$b_\alpha = b_{\alpha,\infty}\exp\left(\frac{E_\alpha}{RT}\right),\ \alpha = L,U,H \qquad (6)$$

$$w(p,T) = \left(\frac{\exp\left(\frac{\ln(p) - \ln\left(p_{step}(T)\right)}{\sigma(T)}\right)}{1 + \exp\left(\frac{\ln(p) - \ln\left(p_{step}(T)\right)}{\sigma(T)}\right)}\right)^\gamma \qquad (7)$$

$$\sigma(T) = \chi_1\exp\left(\chi_2\left(\frac{1}{T_0} - \frac{1}{T}\right)\right) \qquad (8)$$

$$p_{step}(T) = p_{step,0}\exp\left(\frac{-H_{Step}}{R}\left(\frac{1}{T_0} - \frac{1}{T}\right)\right) \qquad (9)$$

The methanol uptake at a certain pressure and temperature *X(p,T)* is calculated from two Langmuir-terms (X_L and X_U), representing the adsorption before and after the step in the uptake. *w(p,T)* is a weighting function that depends on the pressure *p*, the temperature *T* and the pressure p_{step} at which the uptake step occurs. Further symbols X_∞, b_α, E_α and $\chi_{1,2}$ represent fit parameters.[2,3]

COP calculation

The coefficient of performance (COP) for cooling can be defined as the ratio of evaporation enthalpy of the liquid phase and consumed heat for the desorption process:[4,5]

$$COP_C = \frac{Q_{evap}}{Q_{des} + Q_{IH}} \qquad (10)$$

In the numerator the evaporation enthalpy of methanol is used (34.4 kJ/mol). In the denominator the amounts of heat to apply for desorption (Q_{des}) and isosteric heating (Q_{IH}) of the adsorbent are added.

$$COP_{\mathrm{H}} = \frac{Q_{\mathrm{ads}} + Q_{\mathrm{cond}} + Q_{\mathrm{IC}}}{Q_{\mathrm{des}} + Q_{\mathrm{IH}}} \tag{11}$$

In the numerator the amounts of usable heat are summed up. It is the heat of adsorption (Q_{ads}), the heat from condensation (Q_{cond}) and the heat from isosteric cooling (Q_{IC}). In the denominator the amounts of heat to apply for desorption (Q_{des}) and isosteric heating (Q_{IH}) of the adsorbent are summarized.

The amounts of heat can be calculated from energy balances:

$$\mathrm{d}Q_{\mathrm{IH}} = m_{\mathrm{ads}} \cdot \left(c_{\mathrm{p,ads}} + X_{\mathrm{max}}\, c_{\mathrm{p,fl}}\right)\mathrm{d}T \tag{12}$$

$$\mathrm{d}Q_{\mathrm{des}} = m_{\mathrm{ads}} \cdot \left(c_{\mathrm{p,ads}} + X(p,T) c_{\mathrm{p,fl}}\right)\mathrm{d}T - m_{\mathrm{ads}} q_{\mathrm{st}}(T)\mathrm{d}X \tag{13}$$

$$Q_{\mathrm{evap}} = m_{\mathrm{ads}} \cdot \left(\Delta h_{\mathrm{vap}}(T_{evap}) - c_{\mathrm{p,g}}\left(\overline{T} - T_{\mathrm{evap}}\right)\right)\left(X_{\mathrm{max}} - X_{\mathrm{min}}\right) \tag{14}$$

$$\mathrm{d}Q_{\mathrm{ads}} = m_{\mathrm{ads}} \cdot \left(c_{\mathrm{p,ads}} + X(p,T) c_{\mathrm{p,fl}}\right)\mathrm{d}T - m_{\mathrm{ads}} q_{\mathrm{st}}(T)\mathrm{d}X \tag{15}$$

$$\mathrm{d}Q_{\mathrm{IC}} = m_{\mathrm{ads}} \cdot \left(c_{\mathrm{p,ads}} + X_{\mathrm{max}}\, c_{\mathrm{p,fl}}\right)\mathrm{d}T \tag{16}$$

$$Q_{\mathrm{cond}} = m_{\mathrm{ads}} \cdot \left(\Delta h_{\mathrm{vap}}(T_{evap}) - c_{\mathrm{p,g}}\left(\overline{T} - T_{\mathrm{evap}}\right)\right)\left(X_{\mathrm{max}} - X_{\mathrm{min}}\right) \tag{17}$$

Herein m_{ads} refers to the adsorbent mass, $c_{\mathrm{p,ads}}$, $c_{\mathrm{p,fl}}$ and $c_{\mathrm{p,g}}$ to the isobaric heat capacities of adsorbent, water and water vapor, $\overline{T}$ to the arithmetic mean temperature during desorption.

$$\overline{T} = 0.5\left(T_{\mathrm{des,max}} + T_{\mathrm{des,min}}\right) \tag{18}$$

Using the before described set of equations, the COP for a heat pump cycle was calculated for a heating temperature of 40 °C, and desired cold temperature of 10 °C and a variation of driving temperatures lower than 95 °C. As suggested by de Lange et al. and for the sake of comparability, the capacity of the adsorbent $c_{\mathrm{p,ads}}$ was assumed to 1 kJ/kg.[9]

REFERENCES

1 H. Reinsch, R. S. Pillai, R. Siegel, J. Senker, A. Lieb, G. Maurin and N. Stock, *Dalton Trans.*, 2016, **45**, 4179-4186.

2 M. Hefti, L. Joss, Z. Bjelobrk and M. Mazzotti, On the Potential of Phase-Change Adsorbents for CO_2 Capture by Temperature Swing Adsorption. *Faraday Discuss.*, 2016, **192**, 153–179.

3 S.-J. Ernst, M. Baumgartner, D. Fröhlich, H.-J. Bart and S. K. Henninger, Adsorbentien für sorptionsgestützte Klimatisierung, Entfeuchtung und Wassergewinnung. *Chem. Ing. Tech.*, 2017, **89**, 1650–1660.

4 M. F. de Lange, K. J. F. M. Verouden, T. J. H. Vlugt, J. Gascon and F. Kapteijn, Adsorption-Driven Heat Pumps: The Potential of Metal-Organic Frameworks. *Chem. Rev.*, 2015, **115**, 12205–12250.

5 S.-J. Ernst, F. Jeremias, H.-J. Bart and S. K. Henninger, Methanol Adsorption on HKUST-1 Coatings Obtained by Thermal Gradient Deposition. *Ind. Eng. Chem. Res.*, 2016, **55**, 13094–13101.